

QBO and ENSO Variability in Temperature and Ozone from SHADOZ (1998-2005)

S. Lee,¹ D. M. Shelow,¹ A. M. Thompson,¹ S. K. Miller¹

S. Lee, Department of Meteorology, The Pennsylvania State University, 503 Walker Building, University Park, PA 16802, USA. (sl@meteo.psu.edu)

¹Department of Meteorology, The Pennsylvania State University, 503 Walker Building, University Park, PA 16802, USA.

Abstract.

Temperature and ozone profiles from SHADOZ (1998-2005) radiosonde and ozonesonde profiles are analyzed. Data from four representative stations are used to investigate regional differences as well as QBO and ENSO influences on vertically fine structure.

Principal components of the ozone profile time series at Kuala Lumpur ($101^{\circ}E$ $3^{\circ}N$) are adopted as a stratospheric QBO index to study tropospheric temperature and ozone signatures associated with the QBO. A downward propagating QBO ozone signal extends to the mid-troposphere where the phase analysis of the temperature anomalies implies that the driving force is a zonal mean overturning circulation associated with thermal wind adjustment. The maximum tropospheric ozone anomalies associated with the QBO are ≈ 8 ppbv, about 10-20% that of typical tropical tropospheric ozone values, and differ in phase at the four sites. Temperature and ozone fields, linearly regressed against the QBO index, suggest that dynamical processes, including horizontal transport, play an important role in the observed tropospheric ozone anomalies.

Temperature profiles, regressed against the Southern Oscillation Index (SOI), reveal anomalously cool, but also wavy lower stratospheric temperature anomalies over Kuala Lumpur and Nairobi ($37^{\circ}E$ $1^{\circ}S$). Tropospheric ozone profiles associated with the SOI show a statistically significant signal that is consistent with anomalous vertical motions that are known to occur during ENSO, but also exhibit fluctuations at a 40-50 day time scale.

1. Introduction

1 There exist various interannual and intraseasonal dynamical processes that can influence
2 the variability of tropical temperature and ozone. The quasi-biennial oscillation (QBO)
3 is the most prominent form of variability in the tropical stratosphere (Reed et al. 1961;
4 Veryard and Ebdon 1961; Naujokat 1986; Andrews et al. 1987; Reid 1994). Accordingly,
5 the temporal and spatial characteristics of its dynamical and thermodynamical fields
6 (Dunkerton and Delisi 1985; Dunkerton 1990; see Baldwin et al. 2001 for a review),
7 as well as its impact on stratospheric ozone variability have been well documented (see
8 Baldwin et al. 2001 for a review).

9 While the QBO is undoubtedly the dominant form of interannual variability in the
10 tropical stratosphere, the QBO-related tropical tropospheric ozone signal is less well un-
11 derstood. Ziemke and Chandra (1999) estimated the tropospheric column ozone (TCO)
12 from TOMS data, and correlated the TCO values with a QBO index which is based on
13 the EOF analysis by Wallace et al. (1993) and Randel et al. (1995). They found that
14 a statistically significant (see their paper for detail) tropical TCO signal is present be-
15 tween $30^{\circ}W$ and $90^{\circ}E$, and that the TCO at $2.5^{\circ}S$, averaged between $5^{\circ}W$ and $5^{\circ}E$, is
16 negatively correlated with stratospheric column ozone (SCO) three months earlier. This
17 delayed anti-correlation between TCO and SCO is consistent with the idea that the TCO
18 response is due to upper tropospheric ozone photochemistry caused by the stratospheric
19 ozone anomaly. However, because the estimated TCO anomalies are much greater than
20 those predicted by photochemical models, Ziemke and Chandra (1999) concluded that
21 dynamical effects may be a critical factor.

22 For the other prominent tropical variability, the El Niño-Southern Oscillation (ENSO),
23 while its impact on the tropospheric temperature has been documented (e.g., Reid 1994),
24 studies on its influence on the stratospheric temperature are relatively new and recent
25 (e.g., Fernandez et al. 2004; Trenberth and Smith 2006; Garcia-Herrera et al. 2006;
26 Randel et al. 2009). Being focused in the tropics, we are particularly interested in
27 the tropical upper troposphere-lower stratosphere (UT-LS) region. Trenberth and Smith
28 (2006; hereafter TS), using the European Centre for Medium Range Weather Forecasts
29 (ECMWF) reanalysis, known as the 40-yr ECMWF Reanalysis (ERA-40), shows that
30 the tropical UT-LS region is anomalously cold in association with the warm phase of the
31 ENSO. This is consistent with the finding that the Brewer-Dobson (BD) circulation tends
32 to be stronger during the warm ENSO phase, because adiabatic cooling in the tropical
33 stratosphere must strengthen in response to the more intense BD upwelling (Sassi et al.
34 2004; Taguchi and Hartmann, 2006). However, Fig. 3 of TS shows that the UT-LS cooling
35 takes on a vertical structure more complex than the uniform upwelling would produce.
36 Within the tropics, the strongest negative temperature anomaly occurs at ≈ 18 -19 km,
37 but the cold anomaly quickly weakens with height, essentially disappearing between 21-25
38 km.

39 The accumulation of satellite ozone data, most notably the Total Ozone Mapping Spec-
40 trometer (TOMS) data which dates back to 1979, also allowed investigators to examine
41 the ozone variability associated with the ENSO. Performing empirical orthogonal function
42 (EOF) analysis on the monthly mean Merged Ozone Data (MOD) which is comprised of
43 monthly mean TOMS and the Solar Backscatter Ultraviolet instruments, Camp et al.
44 (2003) found that the first two EOFs (75% of the variance) explain the QBO; the third

45 EOF (15% of the variance) can be attributed to variability associated with an interaction
46 between the QBO and annual cycle; and the fourth EOF (3% of the variance) is linked
47 to the El Niño-Southern Oscillation (ENSO). This relationship between ENSO and ozone
48 has been previously studied (Bojkov 1987; Shiotani 1992; Zerefos et al. 1992; Hasebe
49 1993; Randel and Cobb 1994; Kayano 1997; Thompson and Hudson, 1999). Shiotani
50 (1992) and Kayano (1997) found that the total ozone column anomaly field in the tropics
51 is dominated by zonal wave number one, with increased (decreased) ozone concentration
52 over the western (eastern) Pacific where convection is anomalously inactive (active) during
53 the positive ENSO phase. On the ENSO-ozone relationship, the link was attributed to
54 undulation of the tropical tropopause which is caused by convection anomalies associated
55 with the ENSO (Hasebe, 1993).

56 Taking advantage of the SHADOZ (Southern Hemisphere Additional Ozonesondes) net-
57 work, the goal of this study is to complement the previous studies by documenting the
58 tropical ozone and temperature variability, focusing on tropospheric ozone anomalies as-
59 sociated with the QBO, and the UT-LS temperature and ozone anomalies associated with
60 ENSO. The temperature and ozone data analyzed are from four tropical sites (San Cristo-
61 bal, Natal, Nairobi, Kuala Lumpur) of the SHADOZ network (Thompson et al., 2003a).
62 The locations of these sites are indicated in Fig. 1, together with climatological sea surface
63 temperature field and a schematic of the Walker circulation.

64 The paper is organized as follows. Section 2 describes the data and analysis methods.
65 Ozone and temperature variability associated with the QBO are presented in section 3,
66 and those associated with ENSO are reported in section 4. The conclusions follow in
67 section 5.

2. Data

68 The SHADOZ network has collected over 4000 profiles over 14 stations from 1998-2007
69 (Thompson et al., 2003a,b). Figure 1 shows locations of these sites. The ozone measure-
70 ment is made with electrochemical concentration cell ozonesondes (Johnson et al., 2002;
71 Thompson et al., 2003a). At each SHADOZ site, consistent technique is used, bringing
72 the precision of the ozone measurement to 5-7%. Variations in ozonesonde operational
73 methods and instrumentation employed at the SHADOZ sites (Thompson et al., 2003a;
74 Smit et al., 2007; Thompson et al., 2007; Deshler et al., 2008) may introduce slight biases
75 in absolute ozone readings among individual SHADOZ sites (e.g. Fig 9 in Thompson et
76 al., 2003a; Figure 8 in Thompson et al., 2007) but they do not affect the PC and EOF
77 analyses presented here.

78 Ozone and temperature data used in this study were reprocessed in April 2007; a few
79 profiles were corrected or discarded relative to data used in earlier studies (e.g., Thompson
80 et al., 2003a,b; 2007; Folkins et al., 2006; Randel et al., 2007). These data are archived at
81 <http://croc.gsfc.nasa.gov/shadoz>. Temperature and pressure are recorded by standard
82 Vaisala radiosondes, except at Ascension and Natal, where Sippican instruments are used.

83 For the ease of performing the EOF and linear regression analyses used in this study, the
84 above ozone and temperature data were linearly interpolated into a regularly spaced 5-
85 day interval in time and 1-km interval in height. With these interpolated data, a seasonal
86 cycle was calculated. The seasonal cycle was then subtracted from the interpolated data to
87 generate *deseasonalized data*. To isolate interannual variability, this deseasonalized data
88 was subject to a 10-point Butterworth filter whose cut-off period is one year. Throughout
89 this paper, the latter data will be referred to simply as *low-pass data*. The vertical range

90 analyzed is from 1 km to 28 km above the ground. The period covered is from January
91 1, 1998 to December 27, 2005, with the exception of San Cristobal and Natal where the
92 data start on February 24, 1998 and January 26, 1999, respectively.

93 To aid interpretations of the analysis results of the SHADOZ data, we also use zonal and
94 vertical wind data from the global National Center for Environmental Prediction-National
95 Center for Atmospheric Research (NCEP-NCAR) reanalysis dataset (Kalnay et al. 1996).
96 The reanalysis dataset used by this study spans the same time period as the SHADOZ
97 data. The wind fields have been interpolated from sigma to height coordinates using a
98 cubic spline (Son and Lee 2007). The wind fields are then zonally and meridionally (from
99 $15^{\circ}S$ to $15^{\circ}N$) averaged to obtain a representative vertical wind profile for the tropical
100 stratosphere.

3. QBO signals

3.1. QBO index

101 Following the lead of Wallace et al. (1993) and Fraedrich et al. (1993), we construct
102 a set of QBO indices based on EOF analysis. Unlike these previous studies, however,
103 the EOF analysis in this study is performed on SHADOZ ozone and temperature data,
104 instead of monthly mean zonal winds. The EOF analysis was performed using MATLAB's
105 PRINCOMP routine.

106 For each of the four station data, EOF analysis was performed both for the deseason-
107 alized and low-pass data. Even when all vertical levels are included in the analysis, the
108 stratospheric QBO signal dominates in the first two EOFs and these EOFs explain sub-
109 stantial fractional variance (see Tables 1). Because ozone concentrations are much greater
110 in the stratosphere than in the troposphere, the fractional variance explained by the first

111 two EOFs, the QBO signal, is also greater for the ozone than for the temperature field
112 (see Tables 1 and 3). For the ozone, the combined variance from the deseasonalized data is
113 also very large (between 78-87 %), only about 10 % smaller than that of the low-frequency
114 data. Because the QBO signal occupies a higher fractional variance in the ozone than in
115 the temperature data, the ozone EOFs are better suited for defining the QBO index.

116 The tropospheric profiles in these EOFs are suspect, however, as they indicate vertically
117 uniform tropospheric anomalies for all four sites (not shown). This is not surprising
118 because EOF patterns often fill the entire analysis domain to maximize variance (Richman,
119 1986). That is, if the analysis domain is larger than the phenomenon of interest, there is an
120 increased likelihood that the EOF patterns misrepresent actual structures. To overcome
121 this shortcoming, we repeat the EOF analysis on data limited to the stratosphere, and
122 then look for tropospheric patterns associated with the resulting stratospheric EOF.

123 Figure 2 shows two leading ozone EOFs where the analysis domain is confined to be-
124 tween 20 and 28 km. For all four sites, the two leading EOFs together once again describe
125 the QBO. The EOF1 maximum occurs at about 3-4 km above the EOF2 maximum, with
126 PC1 leading PC2, indicating downward propagation of the temperature and ozone anoma-
127 lies. In addition, as was found previously (Wallace et al. 1993; Fraedrich et al. 1993),
128 the EOF analysis also captures the property that the downward propagation during the
129 westerly phase occurs more rapidly than during the easterly phase: each of the positive
130 PC1 extrema lead subsequent positive PC2 extrema by about 2-3 months, while the nega-
131 tive PC1 extrema lead subsequent negative PC2 extrema by about one year. These QBO
132 characteristics are also evident in the EOFs of the unfiltered data (the thin curves in Fig.
133 2). Although the fractional variances accounted for by EOF1 and EOF2 (see Table 3)

134 are greater for low-pass filtered data, those for the unfiltered data are also substantial.
135 Comparison between Tables 1 and 3 indicates also that the difference in fractional vari-
136 ance between EOF1 and EOF2 is smaller for the analysis confined to the stratosphere,
137 reflecting the fact that the cyclic QBO signal is confined mostly to the stratosphere.

138 As can be seen in Fig. 2, the first two EOFs from all four SHADOZ sites under
139 consideration show a robust stratospheric QBO signal. Therefore, any one of the four sets
140 of the two leading PCs can be used as a QBO index. Because Kuala Lumpur is closest to
141 Singapore, the most prominent historical site for QBO observations, we choose the two
142 leading PCs from the low-pass ozone data at the Kuala Lumpur site as our QBO index.
143 For the sake of brevity, the first PC will be referred to as QBO index 1 (QBOI-1), and
144 the second PC as QBO index 2 (QBOI-2).

145 Because this definition of QBO is unconventional, before presenting analysis results, we
146 also show in Fig. 2 two leading temperature EOFs and the corresponding PCs, where
147 the analysis domain is again confined to between 20 and 28 km. For temperature, this
148 confinement substantially raises the combined fractional variances (compare Tables 2 and
149 4). Except for Natal, the temperature PCs closely resemble the corresponding ozone PCs,
150 indicating that the ozone EOF1 (EOF2) profile occurs concurrently with temperature
151 EOF1 (EOF2) profile. Comparing these EOFs, it can be seen that anomalously high
152 (low) ozone concentration roughly coincides with anomalously warm (cold) air. This rela-
153 tionship between ozone and temperature anomalies is consistent with the findings by Choi
154 et al. (2002) and Ribera et al. (2004) who respectively showed that ozone concentration
155 and temperature are anomalously high in the westerly shear zone. Further discussion on

156 the relationships amongst ozone, temperature, and zonal wind will be revisited in Section
157 3.3.

3.2. Temperature anomalies

158 With the QBO index defined above, we then perform linear regression analysis to find
159 temperature anomaly patterns associated with the QBO. Figure 3 shows temperature
160 anomalies regressed against QBOI-1 (left column) and QBOI-2 (right column), at an
161 interval of 70 days which corresponds to 1/12 of the QBO cycle. The negative lags
162 indicate that the QBOI leads the temperature anomalies, and vice versa for positive lags.
163 Because QBOI-2 lags QBOI-1 by 1/4 of the QBO cycle, if the QBOI-1 and QBOI-2
164 describe a perfect sinusoidal cycle with an 840-day period, the lag +210-day regression
165 pattern against QBOI-1 would be identical to the lag 0-day regression pattern against
166 QBOI-2. For ease of comparison, the phase of the QBO is indicated in each panel, where
167 phase 0 is defined as lag 0 of QBOI-1. For the phases that overlap between the left and
168 right columns in Fig. 3, while not identical, the regressed temperature anomaly patterns
169 do indeed closely resemble each other (not shown). Therefore, for conciseness, the phases
170 between $-4\pi/12$ and $\pi/12$, as displayed in Fig. 3, are obtained from linear regression
171 against QBOI-1, and those between $2\pi/12$ and $7\pi/12$ are from linear regression against
172 QBOI-2. The same plotting format was used to construct Figs. 4 and 5.

173 In addition to the expected downward QBO signal in the stratosphere, Fig. 3 shows
174 tropospheric temperature anomaly patterns that exceed the 90% confidence level for a
175 one-sided t-test. During $-4\pi/12 - -2\pi/12$ part of the cycle, (top three rows of the
176 first column) when the negative stratospheric temperature peaks at 20-22 km, positive
177 tropospheric temperature anomalies are seen in all four stations. Except for the San

178 Cristobal site, temperature evolution during this time period hints at the presence of
 179 downward propagation of the temperature anomalies within the troposphere. A half cycle
 180 later, during the period of $2\pi/12 - 4\pi/12$ (the top three rows in the right column in Fig.
 181 3), the temperature anomaly sign reverses, and positive temperature anomalies are found
 182 in the troposphere. Given that this tropospheric temperature signal is associated with
 183 the QBO, and that they occur in unison in all four sites, the tropospheric temperature
 184 anomalies are most likely driven by zonal mean overturning circulation associated with
 185 thermal wind adjustment, as is the case for the stratospheric QBO temperature anomalies.
 186 This implies that there is anomalous tropospheric downwelling during $-4\pi/12 - -2\pi/12$
 187 cycle, and upwelling during $2\pi/12 - 4\pi/12$ cycle of the QBO.

3.3. Stratospheric ozone, temperature, and winds

188 In the stratosphere, the observed ozone anomalies associated with the QBO have been
 189 found to be consistent with the anomaly patterns that would arise if the ozone concen-
 190 tration evolution is dominated by the advection of the climatological mean ozone concen-
 191 tration field by the anomalous vertical wind (Baldwin et al. 2001), that is,

$$\frac{\partial C'_{O_3}}{\partial t} \approx -w' \frac{\partial \bar{C}_{O_3}}{\partial z},$$

192 where C_{O_3} refers to ozone concentration, the overbar denotes the climatological mean, and
 193 the prime is the deviation from the climatological mean. This can explain the occurrence
 194 of high ozone anomaly in the westerly shear zone where $w' < 0$ (Randel and Wu 1996),
 195 although an enhancement in the vertical gradient of the ozone mixing ratio in the westerly
 196 shear zone also plays a role (Choi et al. 2002). Figure 4 shows that this shear- w' -ozone
 197 anomaly relationship also holds for our analysis.

198 The regressed Kuala-Lumpur temperature profiles (Fig. 4) also show positive (negative)
199 anomalies in the westerly (easterly) shear zone (Ribera et al. 2004; Pascoe et al. 2005)
200 where there is anomalous descent (ascent). This is consistent with the expectation that
201 adiabatic warming or cooling causes the QBO temperature anomalies (Gray and Pyle
202 1989; Gray and Dunkerton 1990). However, it has been suggested that ozone heating
203 (Hasebe 1994; Li et al. 1995; Butchart et al. 2003) may also contribute to the production
204 of QBO temperature anomalies. The near in-phase relationship between the ozone and the
205 temperature, as shown in Fig. 4 (see also Figs. 3 and 5), indeed supports this possibility.

3.4. Tropospheric ozone anomalies

206 The regressed ozone field reveals that there are also significant ozone anomalies below
207 the cold point tropopause (see the solid horizontal lines in Figs. 3 and 5), sometimes
208 extending downward anomalies to the 2-km level. The ozone anomalies, corresponding
209 to one standard deviation in the QBOI-1 and QBOI-2 indices, can be as large as 8 ppbv,
210 which is about 10-20% of the typical ozone concentration in the upper troposphere. Figure
211 5 also shows that, unlike for the stratospheric ozone anomalies, the sign changes in the
212 tropospheric ozone anomalies do not occur in unison. Because the stratospheric QBO
213 ozone anomalies are zonally uniform across the sites, this characteristic is inconsistent
214 with the view that the tropospheric ozone anomalies are generated by a UV modulation
215 of upper tropospheric photochemistry, caused by stratospheric QBO ozone anomalies.
216 Tropospheric ozone is also influenced by biomass burning (Thompson et al. 2001) which
217 can be a potential cause for the zonal asymmetry in the tropospheric ozone anomaly.
218 However, because there is no reason to expect that biomass burning is correlated with
219 QBO phases, it is also unlikely that biomass burning is the culprit.

220 Comparing Figs. 3 and 5 once again, amongst all four sites, only the Nairobi tropo-
221 spheric ozone anomalies are consistent with the process represented by $-w' \frac{\partial \bar{C}_{O_3}}{\partial z}$. For
222 Natal and Kuala Lumpur, the regressed tropospheric ozone anomalies take on an oppo-
223 site sign, indicating that other processes need to be taken into account. The advection
224 of anomalous ozone by the climatological vertical wind, $-\bar{w} \frac{\partial C'_{O_3}}{\partial z}$, is unable to explain
225 this discrepancy because, over these two sites, the time-mean vertical wind \bar{w} is positive
226 while the sign of $\frac{\partial C'_{O_3}}{\partial z}$ in the UT-LS region is negative during the time period ($-4\pi/12$ -
227 $-2\pi/12$ cycle) when the upper tropospheric ozone at those locations decreases. Similarly,
228 while tropospheric ozone increases ($4\pi/12$ - $2\pi/12$ cycle), the sign of $-\bar{w} \frac{\partial C'_{O_3}}{\partial z}$ is nega-
229 tive. These results indicate that while there are significant tropospheric ozone anomalies
230 associated with the QBO, to explain the tropospheric ozone response, it is necessary to
231 take into account zonal variations and horizontal transports. In particular, it is possible
232 that the wave source that produces the QBO is restricted to certain regions, and that the
233 convection that acts as the wave source may influence the tropospheric ozone.

234 At the San Cristobal site, the tropospheric ozone anomalies associated with the QBO
235 are essentially nil. If vertical transport was the main process for transporting anomalous
236 tropospheric ozone, this observation would be consistent with the weak tropospheric tem-
237 perature signal at that site. However, given the evidence that horizontal transports may
238 play an important role, to understand the QBO-time scale tropospheric ozone anomalies,
239 it would be necessary to perform a thorough analysis of atmospheric circulations in the
240 troposphere, preferably with global data.

4. ENSO signals

241 To analyze SHADOZ temperature and ozone variability associated with the ENSO, we
242 adopt inverted SOI (ISOI, hereafter) as our index. Although it turned out that the third
243 EOFs of both the temperature and ozone profiles contain an ENSO signal (cf. Camp et
244 al. 2003), with anomalously warm troposphere and a positive correlation between the
245 PC3 time series and the ISOI, their stratospheric structure is found to be unrealistic (not
246 shown). This is not surprising, because lower ranked EOFs are constrained to be orthog-
247 onal with higher ranked EOFs, the vertical temperature structure identified by our EOF3
248 is vulnerable to being an artifact of the EOF analysis. Because the two higher ranked
249 EOFs describe the QBO, the stratospheric structure of EOF3 is particularly problematic.
250 For this reason, we use ISOI, rather than the PC3 time series, as our ENSO index. The
251 daily ISOI is sampled at every five days, concurrent with the interpolated SHADOZ data.
252 In addition to this unfiltered ISOI, a low-pass ISOI is also used as an index. As for the
253 QBO index, the cut-off period is again one year. However, our focus is on the intrasea-
254 sonal variability associated with the ENSO (Feldstein 2000; Johnson and Feldstein 2010),
255 because the 8-year period is too short for analyzing the interannual ENSO variability.

4.1. Temperature anomalies

256 To investigate the temperature structure associated with ENSO, a linear regression
257 analysis was performed in which the SHADOZ temperature data was regressed against
258 the ISOI. We first examine temperature fields regressed against the low-pass ISOI (Fig.
259 6). Below 15 km, the atmosphere is anomalously warm overall, with a notable exception
260 at Natal. In this location, given one standard deviation in ISOI, the temperature at 1 km
261 above the ground is almost 7 degrees cooler than climatological mean. At levels above

262 25 km, all four sites show anomalous cooling. Between 15 km and 25 km, temperature
263 anomalies display a wavy structure in the vertical, particularly for Nairobi and Kuala
264 Lumpur; at Nairobi, a local maximum at 19 km is flanked by two local minima, one at
265 17 km and the other at 25 km; at Kuala Lumpur, a local minimum at 18 km is flanked
266 by two local maxima, one at 16 km and the other at 22 km. In addition, there are many
267 station-to-station variations. The inter-station variations in the temperature anomalies
268 between the 15 km and 25 km levels is also hinted at in Fig. 6 of TS. In this figure, the
269 100-hPa temperature anomaly shows significant zonal asymmetry in the tropics, with cold
270 anomalies between the central Pacific and South America and warm anomalies elsewhere.

271 Associated with the aforementioned UT-LS wavy structure, the Kuala Lumpur tem-
272 perature shows a markedly weak cold anomaly between 20 and 25 km and a strong cold
273 anomaly at 18 km. This UT-LS temperature at Kuala Lumpur agrees reasonably well
274 with the tropical UT-LS temperature profile shown by TS's Fig. 3. Because essentially
275 an identical LS feature is present in two different data sets (ERA-40 in TS and SHADOZ
276 in this study) and two different analysis procedures (EOF analysis on temperature field
277 in TS, as opposed to linear regression against ISOI in this study) we conclude that this
278 UT-LS feature is real, and is not due to a deficiency in reanalysis data set or to an artifact
279 of the EOF analysis. Moreover, the zonal variation within the layers between 15 km and
280 25 km (Fig. 6) indicates that this wavy UT-LS temperature anomaly structure does not
281 occur uniformly in the zonal direction. Given that convection is most active over the
282 Indian Ocean and western Pacific, the proximity of Kuala Lumpur to this region suggests
283 that variability from this region is the main contributor to the UT-LS wavy feature.

284 Having shown that the UT-LS temperature anomalies, identified in TS, are also cap-
285 tured by the SHADOZ data, we next attempt to address how these UT-LS anomalies
286 are generated. Figure. 6a shows that, while the UT-LS anomalies are characterized by
287 a wavy structure in the vertical, above the 20-km level, the response is almost zonally
288 symmetric. The zonal uniformity in the tropical LS region was also noted by TS. This
289 vertical and zonal structure does not conform to any known equatorial disturbances. Be-
290 cause these UT-LS anomalies are obtained based on either low-pass ISOI (our analysis) or
291 monthly mean reanalysis data (TS), to test if this UT-LS structure arises from low-pass
292 filtering processes which may mask underlying physical process, we repeat the regression
293 analysis, but this time against the unfiltered ISOI. The result is shown in Fig. 7. In this
294 figure, negative (positive) lags represent the temperature field leading (lagging) the ISOI.
295 Between lag -20 and lag 25 days, there is very little change in the UT-LS temperature
296 profile over San Cristobal and Natal. However, substantial changes occur for Nairobi,
297 and to a lesser degree for Kuala Lumpur. In other words the UT-LS temperature profiles
298 exhibit greater variation in the zonal direction than what Fig. 6a suggests. Between lag
299 -20 and lag 0 days, it can be seen that the wavy temperature anomalies tilt eastward
300 with height (see the thick dashed line in Fig. 7) in the region between Natal and Kuala
301 Lumpur. This feature is reminiscent of vertically propagating equatorial Kelvin waves
302 (Wallace and Kousky 1968), except that the phase is essentially stationary during the
303 20-day period. After the lag 0 day, Nairobi and Kuala Lumpur temperature anomalies
304 undergo changes so that this upward-eastward tilting, wave-like anomaly structure is no
305 longer evident.

306 Upon averaging the composite fields from lag -20 to lag 25 days, we find that the
307 resulting field (Fig. 6b) resembles Fig. 6a, and is again consistent with the findings
308 by TS (see their Figs. 3 and 6). One implication is that the zonal symmetry above
309 20-km level, shown by Fig. 6 and noted by TS, may arise from a time-averaging of wave-
310 like phenomena which undergo spatial and temporal modulations. Because the spatial
311 coverage of the radiosonde data is limited, it is difficult to fully investigate the wave-like
312 structure. However, this finding indicates that in order to better understand tropical
313 UT-LS response to ENSO, it is necessary to examine variabilities whose time scales are
314 shorter than a month. The consistency between the UT-LS structure shown in Fig. 6
315 and the findings by TS suggests that ERA40 data is adequate for such investigations.
316 Accordingly, analyses of shorter-time processes with ERA40 data are planned in the near
317 future.

4.2. Ozone anomalies

318 This subsection presents ozone variability associated with ENSO, once again identified
319 by ozone fields linearly regressed against the ISOI. Figure 8 shows regressed ozone fields
320 associated with the low-pass ISOI. Except over Natal, stratospheric ozone anomalies are
321 overall negative, implying upward transport of low-ozone tropospheric air. Within the
322 troposphere, positive ozone anomalies are seen over Natal and Kuala Lumpur. This
323 result is consistent with anomalous downwelling over these regions. (As a reference for
324 the normal condition, Walker circulation is indicated in Fig. 1.) In the same manner, over
325 Nairobi which is embedded in an anomalous upwelling region, negative ozone anomalies
326 can be seen. Although data from only four stations are analyzed, the results shown in

327 Fig. 8 are consistent with the finding of Kayano (1997) which was based on TOMS data
328 (see their Fig. 9).

329 Except for San Cristobal, the ozone anomalies, in both the troposphere and stratosphere,
330 exhibit substantial changes in amplitude at submonthly time scales (see Fig. 9). For
331 example, the positive tropospheric ozone anomalies over Kuala Lumpur gradually increase
332 from lag -20 days to lag 0 day, and then gradually decrease between lag 0 day and lag 25
333 days. Over Natal, the opposite behavior can be seen, with a decrease during the first half,
334 and an increase during the second half of the lag days. This time scale, about 40-50 days,
335 coincides with that of the Madden-Julian Oscillation (MJO; Madden and Julian 1971,
336 1972). Given that the ENSO is closely linked to MJO (Hendon et al. 2007), we suspect
337 that the intraseasonal time scale of ozone variation seen in Fig. 9 may be associated with
338 MJO. This possibility has been explored by Ziemke and Chandra (2003).

339 It is also worthwhile to note that Natal's 1-km ozone anomalies, as for the temperature
340 anomalies (Figs. 6 and 7), are notably large. Because these large anomalies are transient
341 (see Figs. 7 and 9), and because such a large anomaly does not occur in the fields
342 regressed against the QBO index (see Figs. 3 and 5), we conclude that in all likelihood
343 these anomalies are real and not due to an instrument error. However, we do not yet have
344 an explanation for these large, highly localized anomalies.

5. Concluding remarks

345 Temperature and ozone data from selected SHADOZ stations (San Cristobal, Natal,
346 Nairobi, and Kuala Lumpur) are analyzed to study their variability in the tropics. For
347 both temperature and ozone data, the first two EOFs together are shown to represent the
348 QBO.

349 To study ozone and temperature variability associated with the QBO, a set of QBO in-
350 dices was constructed. For this purpose, an EOF analysis was performed on low-frequency
351 ozone data from Kuala Lumpur, excluding data below 20 km. The resulting first two PCs
352 are then defined as our QBO index. Linear regression analysis with the QBO index is used
353 to investigate tropospheric ozone and temperature profiles associated with the QBO. It
354 was found that the sign of the tropospheric temperature anomaly is zonally uniform, and
355 anticorrelated with lower stratospheric temperature anomalies centered at 20 km, suggest-
356 ing that the tropospheric temperature anomalies are driven by a zonal mean overturning
357 circulation associated with the QBO. In contrast, tropospheric ozone revealed consider-
358 able variability amongst the four sites. This finding is inconsistent with the view that
359 tropospheric ozone anomalies may be caused by a UV modulation of upper tropospheric
360 photochemistry which respond to stratospheric QBO ozone anomalies. In addition, the
361 strong zonal inhomogeneity of the tropospheric ozone anomalies, in the face of the implied
362 (by temperature anomalies) presence of zonally uniform vertical motion, suggests that the
363 tropospheric ozone anomalies, although associated with the QBO, involve dynamical ef-
364 fects that are more complex than that arising from zonally uniform vertical motion. For
365 example, Collimore et al. (2003) showed that the QBO can modulate deep convection in
366 typically convective tropical regions.

367 A regression analysis was also performed against the inverted SOI to investigate tem-
368 perature and ozone variability associated with the ENSO. It was found that stratospheric
369 temperature, as a whole, is anomalously cold. Garfinkel and Hartmann (2007) found that
370 the Arctic stratosphere is warmer (colder) during the warm (cold) phase of the ENSO.
371 This remote response may be explained by a strengthened Brewer-Dobson circulation,

372 induced by increased extratropical Rossby wave breaking during the warm phase of the
373 ENSO (Sassi et al. 2004; Taguchi and Hartmann, 2006). While the overall stratospheric
374 cooling in our study is indeed consistent with this mechanism, this stratospheric cooling
375 also embodies a structure that is oscillatory in the vertical, but much more uniform in the
376 zonal direction.

377 The intraseasonal-scale time evolution of the regression fields reveals a hint of a vertically
378 propagating equatorial Kelvin wave. Consistent with this finding, the method of Pierce
379 and Grant (1998), applied to the SHADOZ dataset, identifies that gravity waves (a Kelvin
380 wave is a type of gravity wave) are most prevalent in the UT-LS region (Thompson et
381 al. 2009). However, a time averaging obscures the wave structure and produces the
382 zonal uniformity. This possibility is also consistent with the findings by Holloway and
383 Neelin (2007) who used satellite and reanalysis data to show that in the tropics there is
384 a conjoined occurrence of tropospheric heating and LS cooling, immediately above the
385 tropopause. These authors explained this LS cooling in terms of internal gravity waves
386 that respond to the tropospheric heating. The LS cooling can also be explained by an
387 upwelling induced by a tropical Rossby wave momentum flux (Boehm and Lee 2003;
388 Norton 2006). Given this variety of probable dynamical processes, detailed analyses with
389 a global data set, such as ERA-40, are needed to gain further knowledge on the UT-LS
390 response to ENSO.

391 It is shown that significant tropospheric ozone anomalies are also found to be associ-
392 ated with ENSO, with positive (negative) anomalies in the region of anomalous down-
393 welling (upwelling). This result is consistent with an earlier analysis based on TOMS data
394 (Kayano 1997). Our analysis further reveals that the ozone anomalies tend to be weaker

395 in the lower troposphere than in the upper troposphere, further supporting that the ozone
396 anomalies are due largely to stratosphere-troposphere exchange processes. Even so, it is
397 noteworthy that the anomaly amplitude (corresponding to one standard deviation of the
398 ISOI) at the 1-km level is as large as 2-4 ppbv over the Natal and Kuala Lumpur sites.

399 In this study, we found that significant QBO and ENSO signals exist in tropospheric
400 ozone. Much of these signals appear to be of dynamic origin at both interannual (for both
401 QBO and ENSO) and intraseasonal (for ENSO) time scales.

402 **Acknowledgments.** SL was supported by the National Science Foundation under
403 Grant ATM-0647776. AMT and SKM were supported by NASA's Aura Validation Pro-
404 gram Grant NNG05GP22G and NNX09AJ23G (M. J. Kurylo, K. W. Jucks). The up-
405 dated and user-friendly SHADOZ data are courtesy of Goddard Space Flight Center, J.
406 C. Witte (SSAI), Archiver.

References

- 407 Andrews, D., J. Holton, and C. Leovy, 1987: *Middle Atmosphere Dynamics*. Academic
408 Press, 489 pp.
- 409 Baldwin, M.P., L.J. Gray, T.J. Dunkerton, K. Hamilton, P.H. Haynes, W.J. Randel, J.R.
410 Holton, M.J. Alexander, I. Hirota, T. Horinouchi, D.B.A. Jones, J.S. Kinnersley, C.
411 Marquardt, K. Sato, and M. Takahashi, 2001: The Quasi-Biennial Oscillation, *Reviews*
412 *of Geophysics*, **39**, 179-229.
- 413 Boehm, M. T., and S. Lee, 2003: The implication of tropical Rossby waves for tropical
414 tropopause cirrus formation and for the equatorial upwelling of the Brewer-Dobson
415 circulation. *J. Atmos. Sci.*, **60**, 247-261.

- 416 Bojkov, R. D., 1987: The 1983 and 1985 anomalies in ozone distribution in perspective.
417 *Mon. Wea. Rev.*, **115**, 2187-2201.
- 418 Butchart, N., A. A. Scaife, J. Austin, S. H. E. Hare, J. R. Knight, 2003: Quasi-biennial
419 oscillation in ozone in a coupled chemistry-climate model. *J. Geophys. Res.*, **108(D15)**,
420 4486, doi:10.1029/2002JD003004.
- 421 Camp, C. D., M. S. Roulston, and Y. L. Yung, 2003: Temporal and spatial patterns
422 of the interannual variability of total ozone in the tropics. *J. Geophys. Res.*, **108**,
423 doi:10.1029/2001JD001504.
- 424 Choi, W., H. Lee, W. B. Grant, J. H. Park, J. R. Holton, K.-M. Lee, and B. Naujokat 2002:
425 On the secondary meridional circulation associated with the Quasi-Biennial Oscillation.
426 *Tellus B*, **54**, 395-406.
- 427 Collimore, C.C., D.W. Martin, M.H. Hitchman, A. Huesmann, and D.E. Waliser, 2003:
428 On The Relationship between the QBO and Tropical Deep Convection. *J. Climate*, **16**,
429 2552-2568.
- 430 Deshler, T., J. Mercer, H.G. J. Smit, B. J. Johnson, S. J. Oltmans, R. Stuebi, G. Levrat,
431 J. Davies, A. M. Thompson, J. Witte, F. J. Schmidlin, G. Brothers, S. Toru, and M.
432 Proffitt, 2008: Balloon Experiment to test ECC-ozonesondes from different manufac-
433 turers, and with different cathode solution strengths: Results of the BESOS flight. *J.*
434 *Geophys. Res.*, **113**, D04307, doi:10.1029/2007JD008975.
- 435 Dunkerton, T.J., 1990: Annual variation of deseasonalized mean flow acceleration in the
436 equatorial lower stratosphere. *J. Meteor. Soc. Japan*, **68**, 499-508.
- 437 Dunkerton, T. J., and D. P. Delisi, 1985: Climatology of the equatorial lower stratosphere.
438 *J. Atmos. Sci.*, **42**, 376-396.

- 439 Feldstein, S. B., 2000: Teleconnections and ENSO: The timescale, power spectra, and
440 climate noise properties. *J. Climate*, **13**, 4430
- 441 Fernandez, N. C., R. G. Herrera, D. G. Puyol, E. H. Martin, R. R. Garcia, L. G. Presa, and
442 P. R. Rodriguez, 2004: Analysis of the ENSO signal in tropospheric and stratospheric
443 temperatures observed by MSU, 1979-2000. *J. Climate*, **17**, 3934-3946.
- 444 Folkins, I., P. Bernath, C. Boone, K. Walker, A. M. Thompson, and J. C. Witte, 2006: The
445 seasonal cycles of O₃, CO and convective outflow at the tropical tropopause. *Geophys.*
446 *Res. Lett.*, **33**, L16802, doi: 10.1029/2006GL026602.
- 447 Fraedrich, K., S. Pawson, and R. Wang, 1993: An EOF analysis of the vertical-time delay
448 structure of the Quasi-Biennial Oscillation. *J. Atmos. Sci.*, **50**, 3357-3365.
- 449 Garcia-Herrera, R., N. Calvo, R. R. Garcia, and M. A. Giorgetta, 2006: Propagation of
450 ENSO temperature signals into the middle atmosphere: A comparison of two general
451 circulation models and ERA-40 reanalysis data. *J. Geophys. Res.*, **111**, D06101, doi:
452 10.1029/2005JD006061.
- 453 Garfinkel, C.I., and D.L. Hartmann (2007), Effects of the El-Nino Southern Oscillation and
454 the Quasi-Biennial Oscillation on polar temperatures in the stratosphere. *J. Geophys.*
455 *Res.*, **112**, D19112, doi:10.1029/2007JD008481.
- 456 Gray, L. J., and J. A. Pyle, 1989: A two-dimensional model of the quasi-biennial oscillation
457 of ozone. *J. Atmos. Sci.*, **46**, 203-220.
- 458 Gray, L. J., and T. J. Dunkerton, 1990: The role of the seasonal cycle in the quasi-biennial
459 oscillation of ozone. *J. Atmos. Sci.*, **47**, 2429-2451.
- 460 Hasebe, F., 1993: Dynamical response of the tropical total ozone to sea surface tempera-
461 ture changes. *J. Atmos. Sci.*, **50**, 345-356.

- 462 Hasebe, F., 1994: Quasi-biennial oscillations of ozone and diabatic circulation in the
463 equatorial stratosphere. *J. Atmos. Sci.*, **51**, 729-745.
- 464 Hendon, H. H., M. C. Wheeler, and C. Zhang, 2007: Seasonal dependence of the MJO-
465 ENSO relationship. *J. Climate*, **20**, 531-543.
- 466 Holloway, C. E., and J. D. Neelin, 2007: The convective cold top and quasi equilibrium.
467 *J. Atmos. Sci.*, **64**, 1467-1487.
- 468 Johnson, B. J., S. J. Oltmans, H. Vömel, T. Deshler, C. Kroger, and H. G. J. Smit, 2002:
469 ECC ozonesonde pump efficiency measurements and sensitivity tests of buffered and
470 unbuffered sensor solutions. *J. Geophys. Res.*, **107**, doi:10.1029/2001JD000557.
- 471 Johnson, N. C., and S. B. Feldstein, 2010: The continuum of North Pacific sea level
472 pressure patterns: Intraseasonal, interannual, and interdecadal variability. *J. Climate*,
473 **23**, 851-867.
- 474 Kalnay et al., 1996: The NCEP/NCAR 40-year reanalysis project. *Bull. Amer. Meteor.*
475 *Soc.*, **77**, 437-470.
- 476 Kayano, M., 1997: Principal modes of the total ozone on the Southern Oscillation
477 timescale and related temperature variations. *J. Geophys. Res.*, **102**, 25797-25806.
- 478 Li, D., K. P. Shine, and L. J. Gray 1995: The role of ozone-induced diabatic heating
479 anomalies in the quasi-biennial oscillation. *Q. J. R. Meteorol. Soc.*, **121**, 937-943.
- 480 Madden, R. A., and P. Julian, 1971: Detection of a 40-50 day oscillation in the zonal
481 wind. *J. Atmos. Sci.*, **28**, 702-708.
- 482 _____, and _____, 1972: Description of global scale circulation cells in the tropics
483 with a 40-50 day period. *J. Atmos. Sci.*, **29**, 1109-1123.

- 484 Naujokat, B. 1986: An update of the observed Quasi-Biennial Oscillation of stratospheric
485 winds over the tropics. *J. Atmos. Sci.*, **43**, 1873-1877.
- 486 Norton, W. A., 2006: Tropical wave driving of the annual cycle in tropical tropopause
487 temperatures. Part II: Model results. *J. Atmos. Sci.*, **63**, 1420-1431.
- 488 Pascoe, C. L., L. J. Gray, S. A. Crooks, M. N. Jukes, and M. P. Baldwin, 2005: The
489 quasi-biennial oscillation: Analysis using ERA-40 data, *J. Geophys. Res.*, 110, D08105,
490 doi:10.1029/2004JD004941.
- 491 Pierce, R. B., and W. B. Grant, 1998: Seasonal evolution of Rossby and gravity wave
492 induced laminae in ozonesonde data obtained from Wallops Island, Virginia, *Geophys.*
493 *Res. Lett.*, 25, 1859-1862.
- 494 Randel, W. J., and J. B. Cobb, 1994: Coherent variations of monthly mean total ozone
495 and lower stratospheric temperature. *J. Geophys. Res.*, **99**, 5433-5447.
- 496 Randel, W. J., F. Wu, J. M. Russell III, J. W. Waters, and L. Froidevaux, 1995: Ozone
497 and temperature changes in the stratosphere following the eruption of Mount Pinatubo,
498 *J. Geophys. Res.*, **100**, 16,753-16,764.
- 499 Randel, W.J., and F. Wu, 1996: Isolation of the ozone QBO in SAGE II data by singular
500 value decomposition. *J. Atmos. Sci.*, **53**, 2546-2559.
- 501 Randel, W. J., M. Park, F. Wu, and N. Livesey, 2007: A large annual cycle in ozone
502 above the tropical tropopause linked to the Brewer-Dobson circulation. *J. Atmos. Sci.*,
503 **64**, 4479-4488.
- 504 Randel, W. J., R. R. Garcia, N. Calvo, and D. Harsh, 2009: ENSO influence on zonal
505 mean temperature and ozone in the tropical lower stratosphere. *J. Geophys. Res. Lett.*,
506 **36**, L15822, doi: 10.1029/2009GL039343.

- 507 Reed, R.G., W.J.Campbell, L.A.Rasmussen and D.G.Rogers, 1961: Evidence of
508 downward-propagating annual wind reversal in the equatorial stratosphere. *J. Geophys.*
509 *Res.*, **66**, 813-818.
- 510 Reid, G. C., 1994: Seasonal and interannual temperature variations in the tropical strato-
511 sphere. *J. Geophys. Res.*, **99**, 18923-18932.
- 512 Ribera et al. 2004: Detection of the secondary meridional circulation associated with the
513 Quasi-Biennial Oscillation. *J. Geophys. Res.*, **109**, D18112, doi: 10.1029/2003JD004363.
- 514 Richman, M. B., 1986: Rotation of principal components. *J. Climatol.*, **6**, 293-335.
- 515 Sassi, F., D. Kinnison, B. A. Boville, R. R. Garcia, and R. Roble, 2004: Effect of El Niño-
516 Southern Oscillation on the dynamical, thermal, and chemical structure of the middle
517 atmosphere. *J. Geophys. Res.*, **109**, D17108, doi:10.1029/2003JD004434.
- 518 Shiotani, M., 1992: Annual, quasi-biennial, and El Niño-Southern Oscillation (ENSO)
519 time-scale variations in equatorial total ozone. *J. Geophys. Res.*, **97**, 7625-7633.
- 520 Smit, H. G. J., W. Straeter, B. J. Johnson, S. J. Oltmans, J. Davies, B. Hoegger, R. Stubi,
521 F. J. Schmidlin, A. M. Thompson, J. C. Witte, I. Boyd, F. Posny, 2007: Assessment
522 of the performance of ECC-ozonesondes under quasi-flight conditions in the environ-
523 mental simulation chamber: Insights from the Juelich Ozone Sonde Intercomparison
524 Experiment (JOSIE). *J. Geophys. Res.*, **112**, D19306, doi: 10.1029/2006JD007308.
- 525 Son, S.-W. and S. Lee, 2007: Intraseasonal variability of the zonal-mean tropical
526 tropopause height. *J. Atmos. Sci.*, **64**, 2695-2706.
- 527 Taguchi, M., and D. L. Hartmann, 2006: Increased occurrence of stratospheric sudden
528 warming during El Niño as simulated by WACCM. *J. Climate*, **19**, 324-332.

- 529 Thompson, A. M., and R. D. Hudson, 1999. Tropical Tropospheric Ozone (TTO) maps
530 from Nimbus-7 and Earth-Probe TOMS by the modified-residual method: Evaluation
531 with sondes, ENSO signals and trends from Atlantic regional time series. *J. Geophys.*
532 *Res.*, **104**, 26,961-26,975.
- 533 Thompson, A. M., J. C. Witte, R. D. Hudson, H. Guo, J. R. Herman, and M. Fujiwara,
534 2001: Tropical tropospheric ozone and biomass burning. *Science*, **291**, 2128-2132.
- 535 Thompson, A. M., et al., 2003a: Southern Hemisphere ADditional Ozonesondes
536 (SHADOZ) 1998- 2000 tropical ozone climatology. 1. Comparison with TOMS and
537 ground-based measurements. *J. Geophys. Res.*, **108**, 8238, doi:10.1029/2001JD000967.
- 538 Thompson, A. M., et al., 2003b: Southern Hemisphere ADditional Ozonesondes
539 (SHADOZ) 1998- 2000 tropical ozone climatology. 2. Tropospheric variability and the
540 zonal wave-one. *J. Geophys. Res.*, **108**, 8241, doi:10.1029/2002JD002441.
- 541 Thompson, A. M., J. C. Witte, H. G. J. Smit, S. J. Oltmans, B. J. Johnson, V.
542 W. J. H. Kirchhoff, and F. J. Schmidlin, 2007: Southern Hemisphere Additional
543 Ozonesondes (SHADOZ) 1998-2004 tropical ozone climatology. 3. Instrumentation, sta-
544 tion variability, evaluation with simulated flight profiles. *J. Geophys. Res.*, **112**, D03304,
545 doi:10.1029/2005JD007042.
- 546 Thompson, A. M., A. L. Loucks, S. Lee, S. K. Miller, and J. C. Witte, 2009: Gravity
547 and Rossby wave influences in the tropical troposphere and lower stratosphere based
548 on SHADOZ (Southern Hemisphere Additional Ozonesondes) Soundings, 1998-2007.
549 Submitted to *J. Geophys. Res.*, doi:10.1019/2009JD013429.
- 550 Trenberth, K. E., and L. Smith, 2006: The vertical structure of temperature in the tropics:
551 different flavors of El Nino. *J. Climate*, **19**, 4956-4970.

- 552 Veryard, R.G. and R.A.Ebdon, 1961: Fluctuations in tropical stratospheric winds. *Met.*
553 *Mag.*, **90**, 125-143.
- 554 Wallace, J. M., and V. E. Kousky, 1968: Observational evidence of Kelvin waves in the
555 tropical stratosphere. *J. Atmos. Sci.*, **25**, 900-907.
- 556 Wallace, J. M., R. L. Panetta, and J. Estberg, 1993: Representation of the equatorial
557 stratospheric quasi-biennial oscillation in EOF phase space. *J. Atmos. Sci.*, **50**, 1751-
558 1762.
- 559 Zerefos, C. S., A. F. Bais, I. C. Ziomas and R. D. Bojkov, 1992: On the relative im-
560 portance of Quasi-Biennial Oscillation and El Nino/Southern Oscillation in the revised
561 Dobson total ozone records. *J. Geophys. Res.*, **97**, 10135-10144.
- 562 Ziemke, J. R., and S. Chandra, 1999: Seasonal and interannual variabilities in tropical
563 tropospheric ozone. *J. Geophys. Res.*, **104**, 21425-21442.
- 564 Ziemke, J. R., and S. Chandra, 2003: A Madden-Julian Oscillation in tropospheric ozone,
565 *Geophys. Res. Lett.*, **30**(23), 2182, doi:10.1029/2003GL018523

	EOF1	EOF2	EOF1+EOF2
Nairobi (36.8°E, 1.3°S)	56.33/67.75	26.12/26.66	82.45/94.41
Kuala Lumpur (101.7°E, 2.7°N)	55.08/67.71	23.47/23.14	78.55/90.85
San Cristobal (89.6°E, 0.9°S)	63.94/72.72	19.75/18.54	83.69/91.26
Natal (35.4°E, 5.4°S)	73.11/79.01	13.44/14.64	86.55/93.65

Table 1. Percentage variances, VAR_d and VAR_l , respectively, explained by EOFs derived from deseasonalized and low-pass ozone profiles. The table displays VAR_d/VAR_l .

	EOF1	EOF2	EOF1+EOF2
Nairobi (36.8°E, 1.3°S)	29.29/45.74	23.04/36.43	52.33/82.17
Kuala Lumpur (101.7°E, 2.7°N)	30.47/48.24	22.42/34.13	52.89/82.37
San Cristobal (89.6°E, 0.9°S)	28.26/40.28	25.07/37.43	53.33/77.71
Natal (35.4°E, 5.4°S)	30.96/50.61	20.75/33.63	51.71/84.24

Table 2. Percentage variances, VAR_d and VAR_l , respectively, explained by EOFs derived from deseasonalized and low-pass temperature profiles. The table displays VAR_d/VAR_l .

	EOF1	EOF2	EOF1+EOF2
Nairobi (36.8°E, 1.3°S)	49.21/62.80	33.89/34.47	83.10/97.27
Kuala Lumpur (101.7°E, 2.7°N)	45.62/60.34	35.03/32.92	80.65/93.26
San Cristobal (89.6°E, 0.9°S)	55.24/66.07	29.08/28.32	84.32/94.39
Natal (35.4°E, 5.4°S)	63.79/73.19	20.59/23.17	84.38/96.36

Table 3. Percentage variances, VAR_d and VAR_l , respectively, explained by EOFs derived from deseasonalized and low-pass ozone profiles above 20 km. The table displays VAR_d/VAR_l .

	EOF1	EOF2	EOF1+EOF2
Nairobi (36.8°E, 1.3°S)	45.94/64.26	27.86/31.92	73.80/96.18
Kuala Lumpur (101.7°E, 2.7°N)	45.94/73.13	27.86/21.14	73.80/94.27
San Cristobal (89.6°E, 0.9°S)	46.57/72.08	27.32/17.76	73.89/89.84
Natal (35.4°E, 5.4°S)	44.09/80.01	29.32/11.81	73.41/91.82

Table 4. Percentage variances, VAR_d and VAR_l , respectively, explained by EOFs derived from deseasonalized and low-pass temperature profiles above 20 km. The table displays VAR_d/VAR_l .

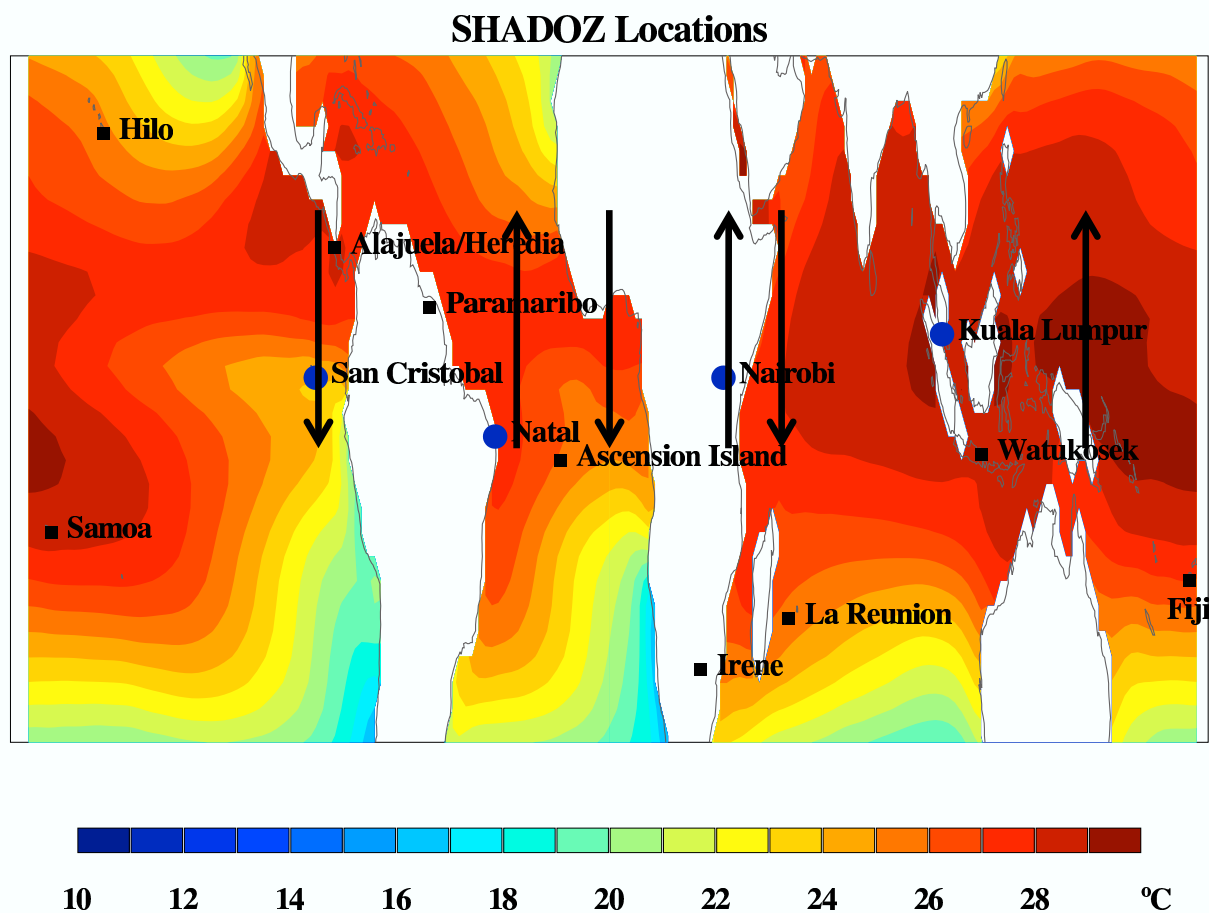


Figure 1. The SHADOZ sites superimposed on the National Oceanic and Atmospheric Administration (NOAA) Extended Reconstructed Sea Surface Temperature version 3 (ERSST v3). Also superimposed is a schematic of climatological Walker circulation: upward (downward) arrows denote rising (sinking) motion. The four SHADOZ sites used for this study are indicated by blue dots.

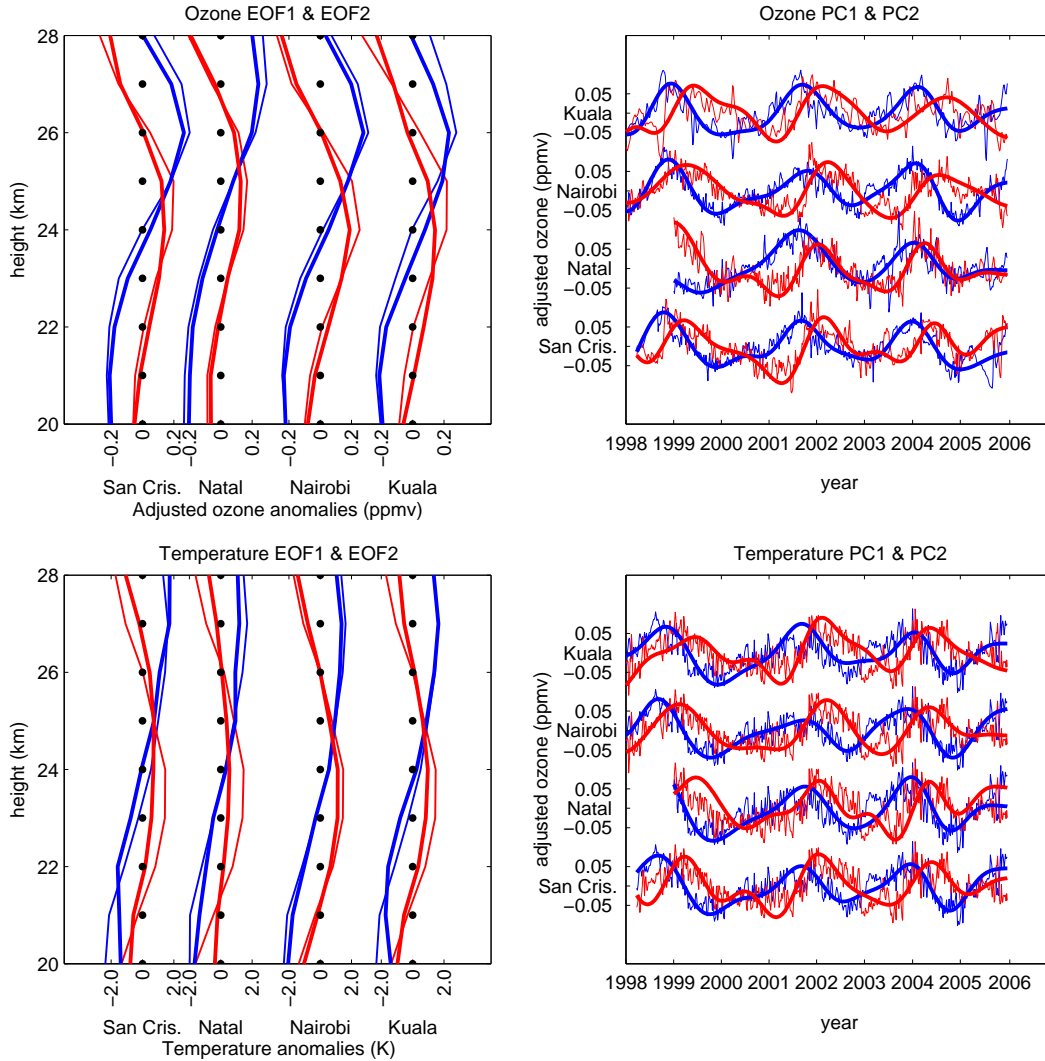


Figure 2. The first two EOFs (left panel) and corresponding PCs (right panel) of ozone (top) and temperature (bottom) data, from Jan. 5, 1998 to Dec. 31, 2005, for San Cristobal, Natal, Nairobi, and Kuala Lumpur. For each site, the first (second) EOF and PC are blue (red); thin (thick) lines are for EOFs and PCs derived from the deseasonalized (low-pass) data. The EOFs are scaled by one standard deviation of the corresponding PC. The distance between individual stations in the plot is roughly proportional to the actual distance between the stations. The regularly spaced dots in the left panels indicate the locations of the interpolated data.

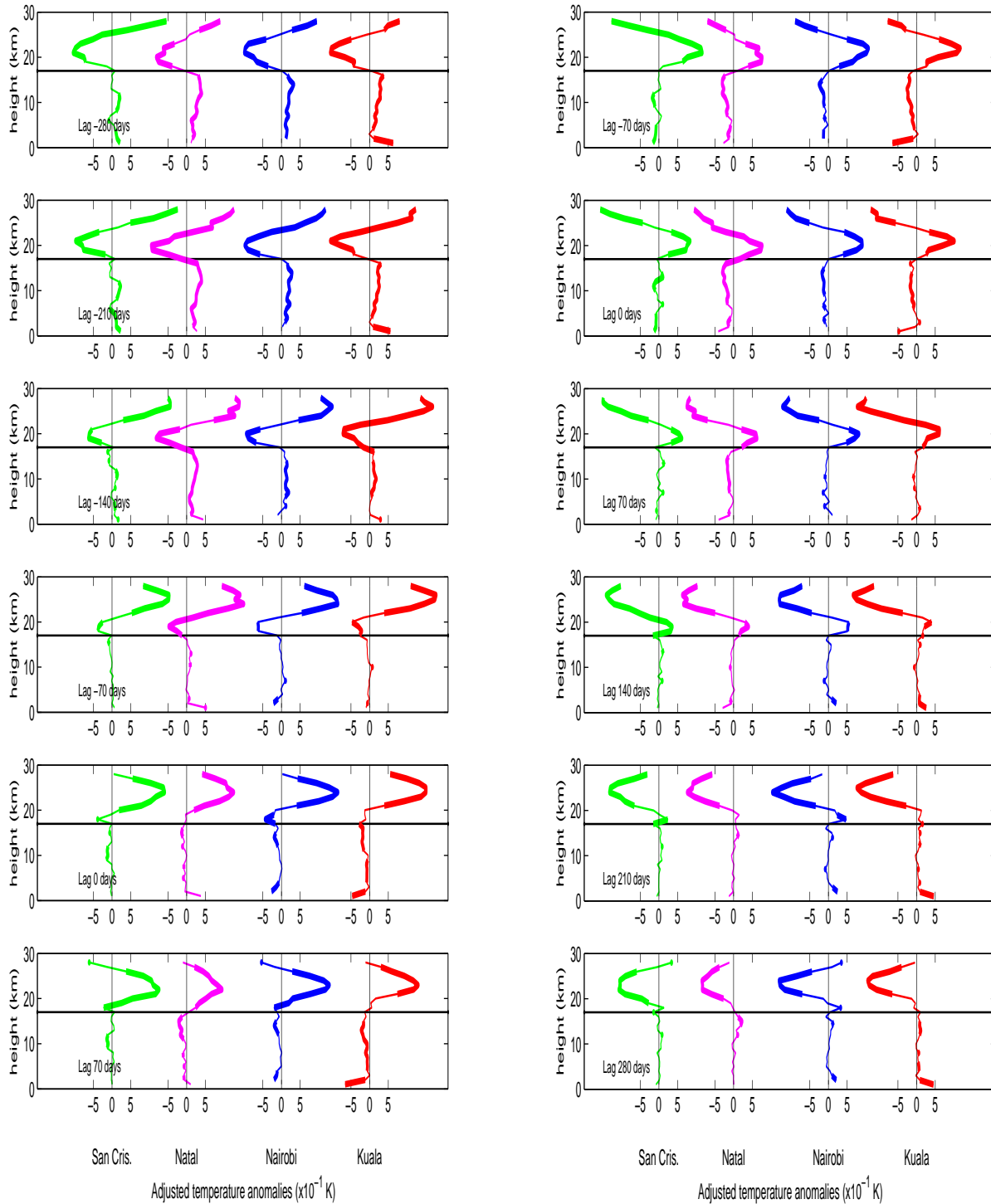


Figure 3. Temperature profiles linearly regressed against QBOI-1 (left column) and QBOI-2 (right column). The bolded regions of the profiles represent values that exceeds the 90% confidence level. The horizontal line in each panel indicates 17-km level, the typical height of the cold point tropopause.

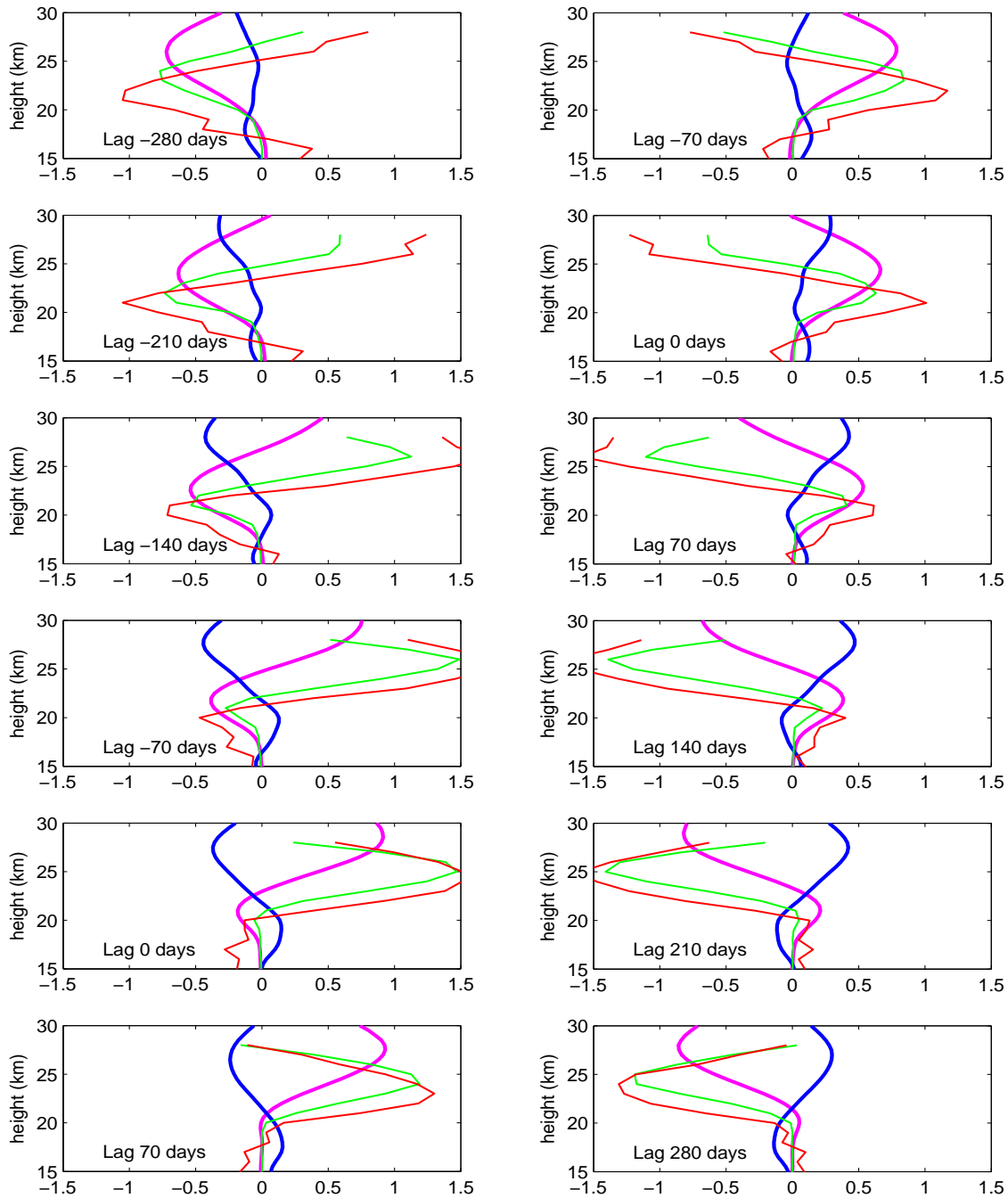


Figure 4. As in Fig. 3, except that the regressed field is Kuala Lumpur ozone mixing ratio (green; $\times 0.2$ ppmv), Kuala Lumpur temperature (red; K), tropical mean zonal wind (magenta; $\times 0.2$ ms^{-1}), and tropical mean vertical wind (blue; $\times (1. \times 10^{-6} ms^{-1})$).

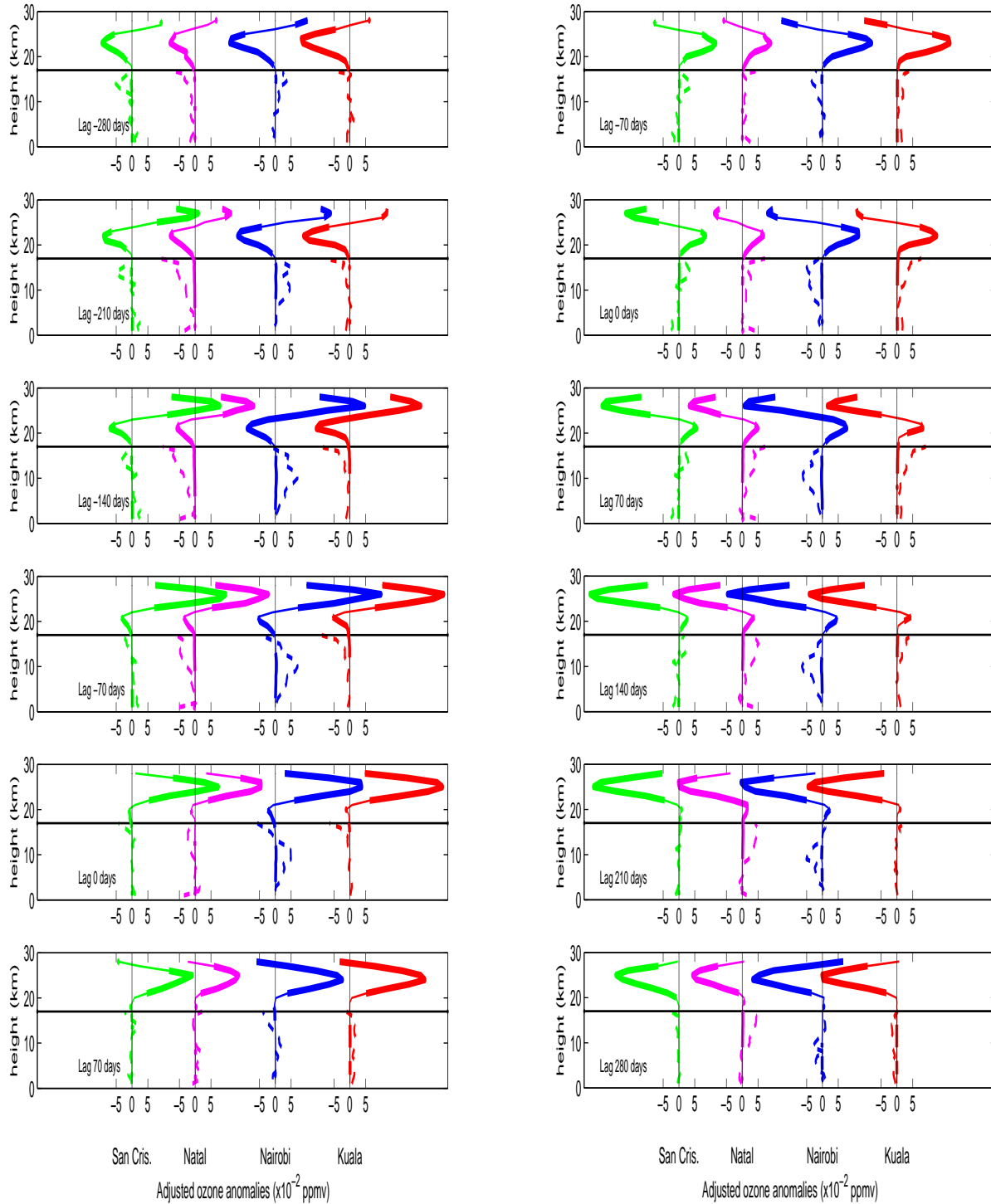


Figure 5. As in Fig. 3, except that the regressed field is ozone. Below 17 km, the dashed profiles are in ppbv.

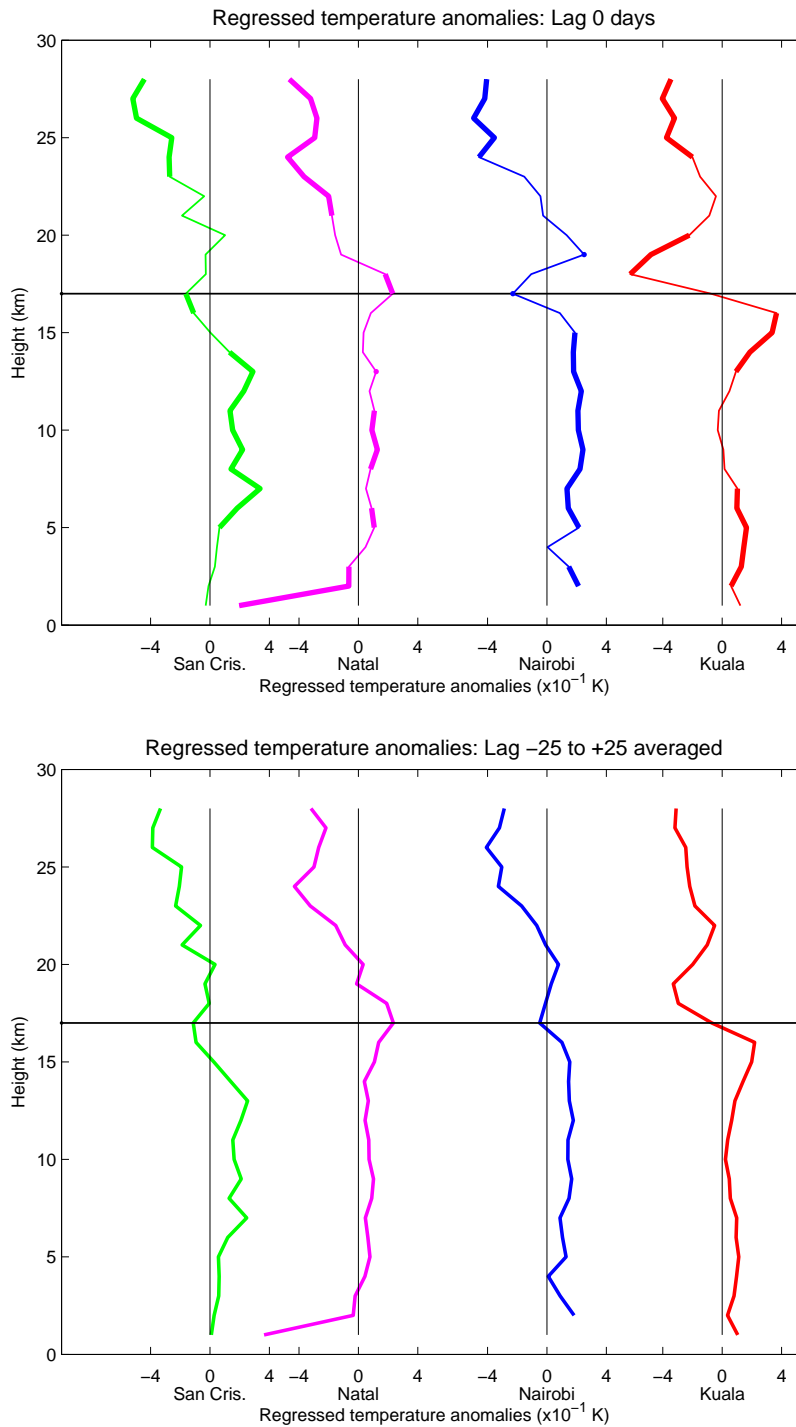


Figure 6. Temperature profiles (a) regressed against low-pass filtered ISOI, and (b) from an average of regressed temperature values that are obtained by regressing against deseasonalized ISOI. The period of averaging ranges from lag -25 to lag 25 days. See the text and Figure 5. In (a), the bolded regions of the profiles represent values that exceeds the 90% confidence level.

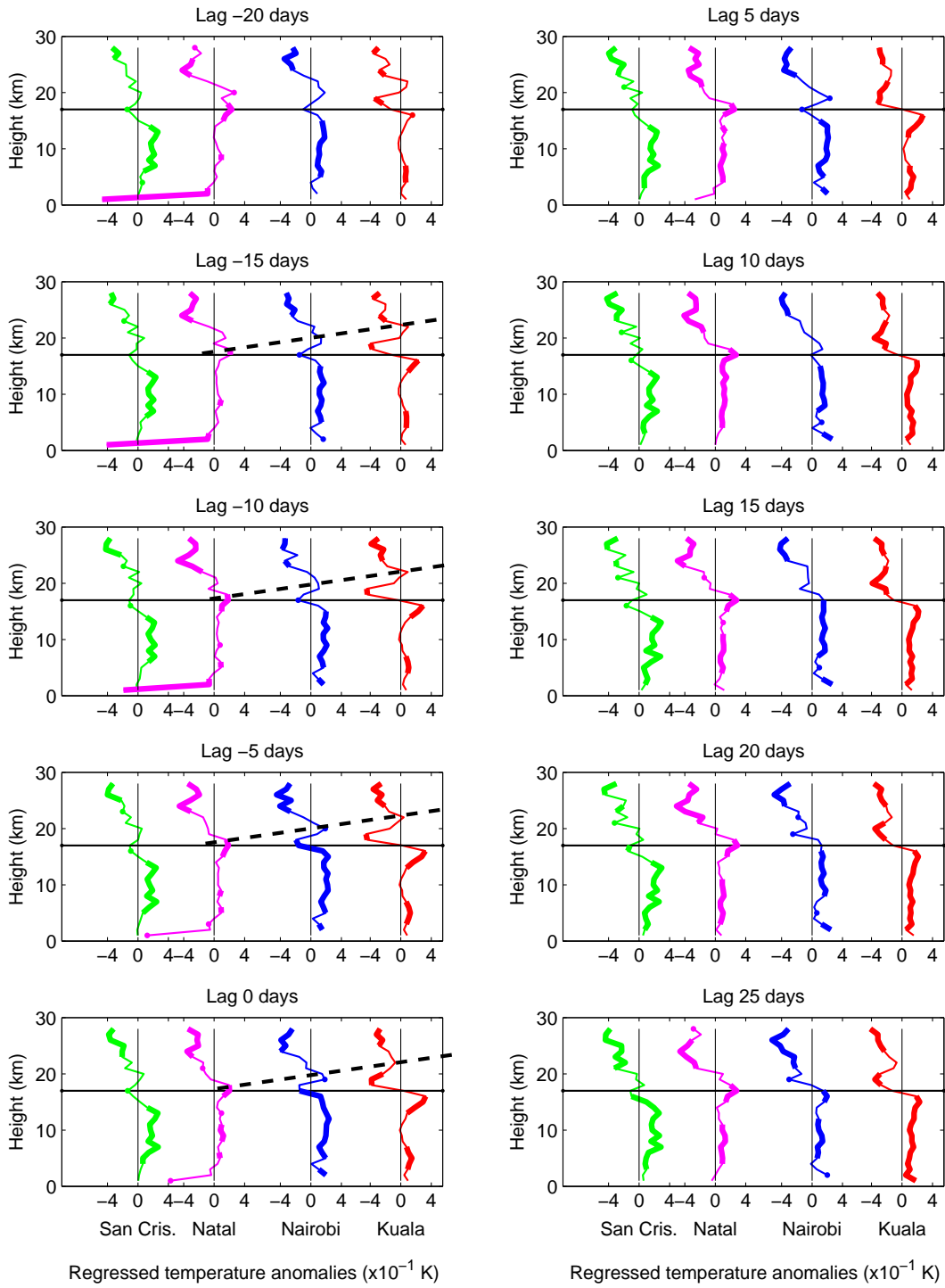


Figure 7. As in Fig. 3, except that the temperature is regressed against deseasonalized ISOI.

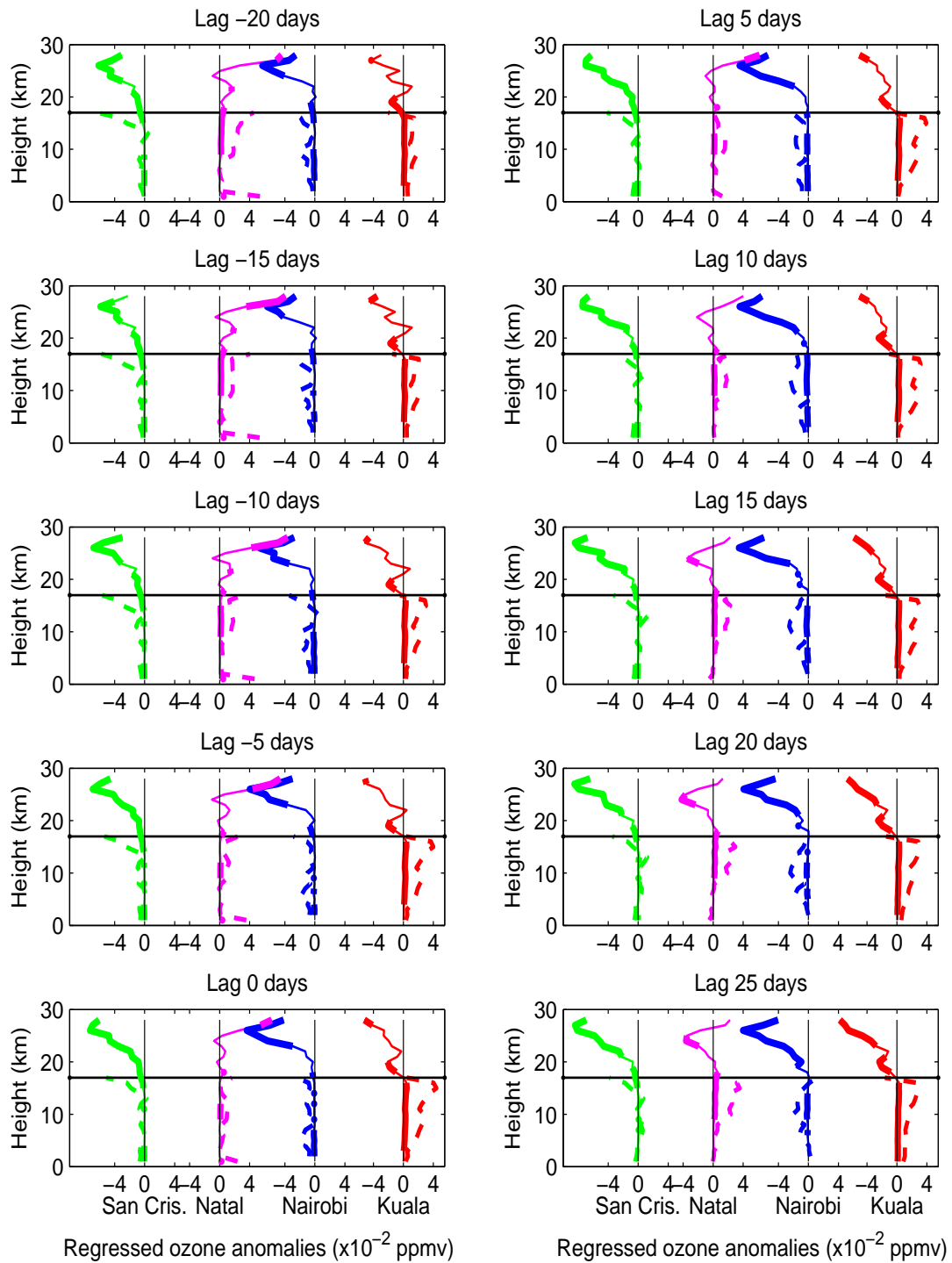


Figure 8. As in Fig. 5, except that the ozone is regressed against deseasonalized ISOI.

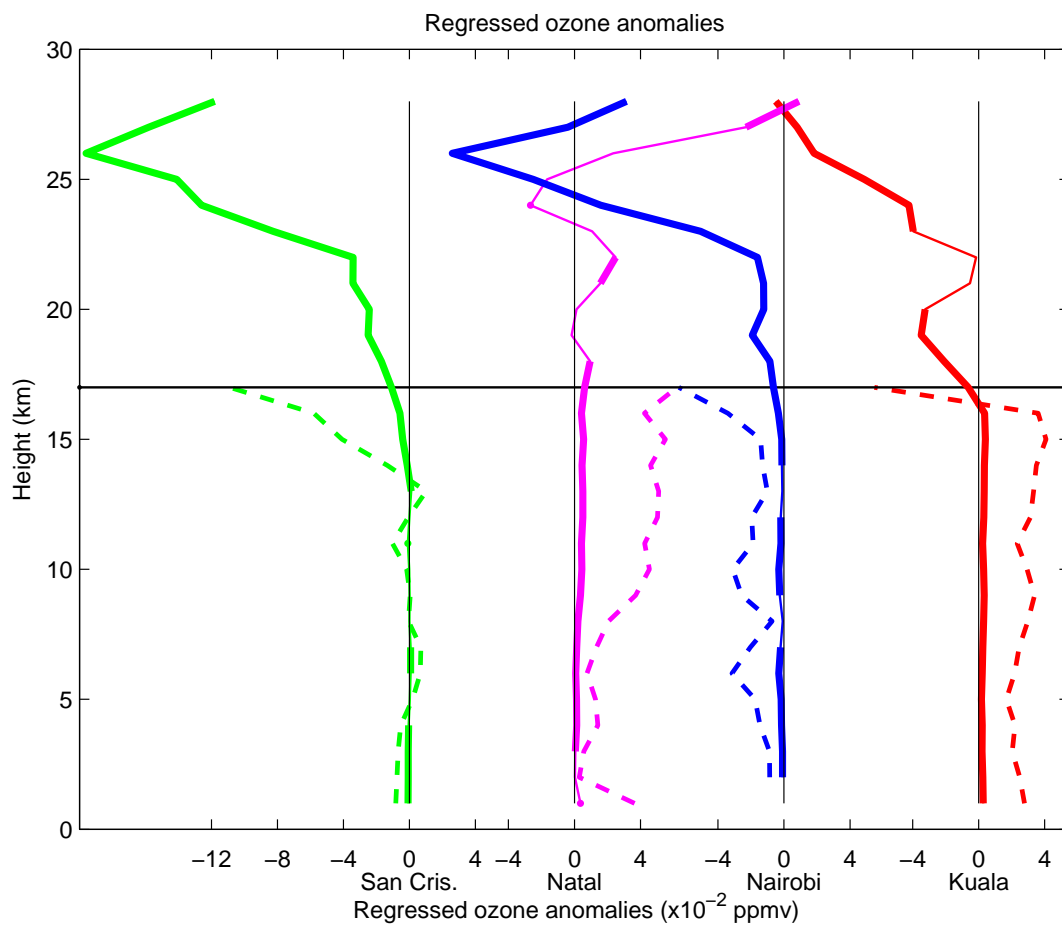


Figure 9. As in Fig. 8, except that the ozone is regressed against low-pass ISOI.